Cardiac Anatomical and Electrical Axes: Proposed Definitions and Interplay

Mohammad Kayyali[1], Ana Mincholé[2], Shuang Qian[1], Alistair Young[1], Devran Ugurlu[1], Elliot Fairweather[1], Steven Niederer[3], John Whitaker[1], Martin Bishop[1], Pablo Lamata[1]

[1]Department of Biomedical Engineering, King's College London, London, UK
[2]BSICoS, I3A, IIA Aragon, University of Zaragoza, Zaragoza, Spain
[3]Imperial College London, London, UK

Abstract

The influence of heart size, position and orientation within the torso on ECG morphology is well-established. Yet, there remains a gap in quantifying and accounting for the impact of this relationship on the ECG biomarkers extracted, presenting an opportunity for tailoring clinical ranges, thus, improving the reliability and robustness of diagnosis and prognosis of electrophysiological disorders. In this context, the aims of this study are (1) to propose a standardised and robust definition of the electrical and anatomical axes, and (2) to describe their relationship in the undiseased adult population. Multimodal clinical data from the UK Biobank, primarily cardiac MRIs and 12-lead ECGs, was used to generate patient-specific biventricular geometry and vectorcardiograms. Five alternative definitions for the 3D orientation axes of the electrical and anatomical axes were computed, followed by assessment of their mutual alignment. Findings demonstrate that maximal alignment occurs between the anatomical axis derived from the vector connecting the valvular plane centre to the apex, and the electrical axis defined by the maximum QRS dipole magnitude in the vectorcardiogram. Furthermore, the electrical axis orientation displays a wider spread than that of the anatomical axis and has a dominant effect on the coupled axis interplay.

1. Introduction

The morphology of the electrocardiogram (ECG) is intrinsically linked to the underlying cardiac anatomy, including heart size, position, and orientation within the thorax. This relationship arises from the fundamental principle that the ECG measures the potential differences on the body surface that represent different projections of cardiac activity. This introduces the challenge of interpreting variations in the ECGs that are due to anatomical variability and not pathology, or vice versa.

While in-silico approaches offer significant insights into the impact of cardiac anatomy on measured variables like QRS duration and wave amplitudes [1][2], the translation of these findings into practical applications like biomarker correction remains a challenge. Automated anatomy reconstruction from imaging and holistic electrical activity representations like the vectorcardiogram (VCG) hold significant potential as they facilitate large-scale analysis of personalised anatomy and electrophysiology.

Anatomical and electrical axes serve as representations of the underlying cardiac orientation and electrical activation pattern. Thus, their characterisation is essential for examining the anatomical-electrical interplay. Traditionally, the anatomical axis has been defined as the long axis of the heart, typically derived manually from imaging data [3], a process that is not only arduous but also often overlooks the right ventricle. On the other hand, most clinical electrical axis derivation relies on Einthoven's triangle [4], an approach that utilises only maximum lead amplitudes and is inherently limited to the frontal plane.

A standardised, robust definition of cardiac anatomical and electrical axes remains elusive. Herein, definitions of axes were generated and evaluated, and their distributions were studied in a cohort of undiseased individuals from the UK Biobank. The definitions maximising mutual 3D alignment between anatomical and electrical axes were proposed as a standard.

2. Methods

2.1. Clinical data & study population

A cohort of 5,000 subjects was studied, each with paired C-MRI scans and 12-lead ECGs. Using nnU-net architecture, the biventricular anatomy was automatically segmented at the end diastolic phase [5]. Surface meshes were then constructed via an atlas-based pipeline and key anatomical regions labelled, including each of the four valves and the left and right ventricles [6].

ECGs with QRS amplitude larger than ±3 SD of the mean for each lead were excluded, as in [7]. Of the remaining 4,769 subjects, 3,080 subjects with no cardiovascular disease history were identified using ICD-10 diagnoses. Table 1 shows the cohort's baseline metrics.

Table 1. Baseline characteristics of undiseased cohort.

Metric	N = 3080
Age, mean ± SD	64.6 ± 7.77
Gender (Female), n (%)	1636 (53%)
BMI (kg/m^2), mean ± SD	26.3 ± 4.25
QRS duration (ms), mean ± SD	88.3 ± 13.9
LV End Diastolic Volume (ml), mean ± SD	139.3 ± 45.8

2.2. Anatomical axis computation

Principal Component Analysis (PCA) was employed in conjunction with labelled regions to derive five distinct orientation axes for each biventricular anatomy.

PCA was applied to the point cloud of surface mesh data to compute two axes of inertia: one for the left ventricle exclusively $(PC1_{LV})$ and another encompassing both the left and right ventricles $(PC1_{LRV})$. Then, spatial centres corresponding to various valve combinations were computed to establish a virtual base. The apex was then defined as the furthest point from this base, located on the left ventricular endocardium. The orientation axis was defined as the vector from the apex to the base with the following configurations:

i. Centre of mitral valve to apex *(MVA)*
ii. Centre of mitral and aortic valves to apex *(MAVA)*
iii. Centre of valve plane to apex *(VPA)*

2.3. Electrical axis computation

The 10-second digital 12-lead ECGs, with a sampling frequency of 500 Hz and an amplitude resolution of 1 µV, were stored in an .xml file alongside automatically computed ECG metrics. During data acquisition (GE Cardiosoft v6), all ECGs underwent low-pass filtering at 100 Hz, high-pass filtering at 0.1 Hz, and a 50 Hz power-line noise filtering. Therefore, no additional preprocessing was performed.

After extracting the median beat of the 12-lead ECG, the Kors transformation matrix was used to construct the three orthogonal leads comprising the corresponding vectorcardiogram (VCG) [8]. This method provides alignment with Frank's orthogonal lead system, V_x, V_y, and V_z. The VCG comprises dipole magnitude, polarity and direction considerations that are not available from a scalar method like the ECG, which only shows the component magnitude along a certain lead axis. The QRS complex was the focus of the study as it has the most diverse morphology variation. The QRS VCG loop was isolated using QRS onset and offset times, computed during acquisition. 5 orientation axes were computed, capturing changes of the dipole's orientation and magnitude during ventricular depolarisation, shown in Figure 1.

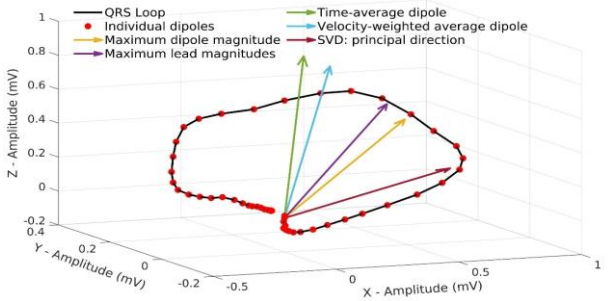

Figure 1. 3D QRS loop with the 5 electrical axis definitions.

The dipole magnitude was calculated at each time point from the three leads as: $({V_x}^2 + {V_y}^2 + {V_z}^2)^{1/2}$. The dipole with maximum magnitude was identified $(maxQRS)$. A vector $(maxXYZ)$ was constructed using each lead's maximum amplitude. The mean QRS dipole was also calculated $(meanQRS)$. To account for variations in dipole velocity along the loop (shown by changing distances between consecutive dipoles), a velocity-weighted average dipole $(v - avgQRS)$ was computed. Lastly, singular value decomposition (SVD) was applied on the matrix of x, y, z data, after centring about the mean. The primary direction $(eig1QRS)$ was regarded as the eigenvector linked to the first eigenvalue of the correlation matrix. Each dipole's unit vector was used as the axis direction.

2.4. Axes analysis

The anatomical-electrical relationship was assessed by different metrics to quantify the alignment between the 25 pairs of anatomical-electrical axes definitions. For true mapping, the VCG coordinate system was rotated to align with that of the DICOM, resulting in the x-axis extending from left to right, the y-axis from anterior to posterior, and the z-axis from inferior to superior. All vectors were assumed to originate at the biventricular centre of mass.

The anatomical-electrical linear relationship of vector sets was studied using an 80(train)/20(test) split of the dataset. For each method pair in the training set, a transformation matrix, T, was derived by solving:

$$Electrical\ vectors = T * Anatomical\ Vectors$$

A linear least squares approach was employed to compute T, minimising the Euclidean norm between predicted (transformed anatomical) and computed electrical vectors. The mean geodesic distance (MGD) between computed and predicted vectors was measured for each of the 25 method pairs using the test data. MGD was chosen as an error metric due to its suitability for comparing directions in 3D, providing a robust measure of angular difference as a discrepancy. By evaluating this error across method pairs, the best pairs were identified based on error minimisation of unseen data.

Moreover, the cosine of the angle between each anatomical-electrical axis pair was computed as a second metric across the cohort. *Spatial consistency* was evaluated using the corresponding standard deviation (SD), with a lower standard deviation indicating higher spatial consistency. Due to the cosine being reflective of only the smallest angle between two vectors in 3D, it does not fully capture the directional variations. Consequently, the angle between each projected vector and the positive horizontal axis was calculated in all 3 anatomical planes. Thus, a direction-dependant angular difference between each anatomical-electrical vector pair was also computed, enabling examination of individual and relative distributions of axes across all three spatial dimensions.

3. Results

3.1. Linear Transformation Errors

The strength of the linear correlation between each anatomical-electrical pair is associated with a lower mean error (geodesic distance between computed and predicted electrical axes). Errors ranged from 1.95 (PC1LV & v-avgQRS) to 0.81 (VPA and eig1QRS), as depicted in Figure 2. The second-best pair emerged as maxQRS and VPA. Notably, a trend of decreasing error is evident with the inclusion of the right ventricle within the anatomical axis computation.

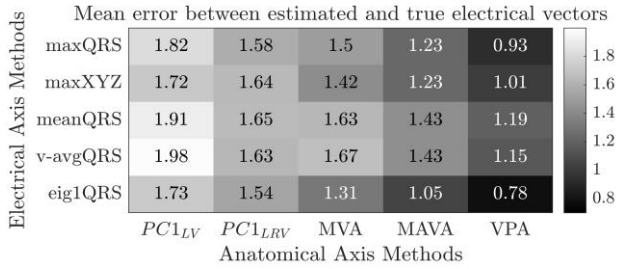

Figure 2. Mean geodesic distance between computed and predicted electrical vectors for anatomical-electrical pairs.

3.2. Angular distributions of axes

The axes pair exhibiting the highest spatial consistency was defined by the VPA anatomical axis and maxQRS electrical axis (see Figure 3), with an SD of 0.19, and the least spatially consistent pair reported an SD of 0.60. Additionally, the VPA anatomical axis also comprised the second lowest SD of 0.21, paired with electrical axis eig1QRS. This agrees with the previous evaluation method, albeit with a reversal in the electrical axis ranking.

Figure 4 highlights that the performance advantage of certain method pairs diminishes when examining the 2D planar angles. It is only in the frontal plane that a visibly higher spatial consistency is observed. Given that the overall spatial consistency was highest in the frontal and transverse planes, a bivariate distribution analysis was performed, illustrated in Figure 5. The spread of the

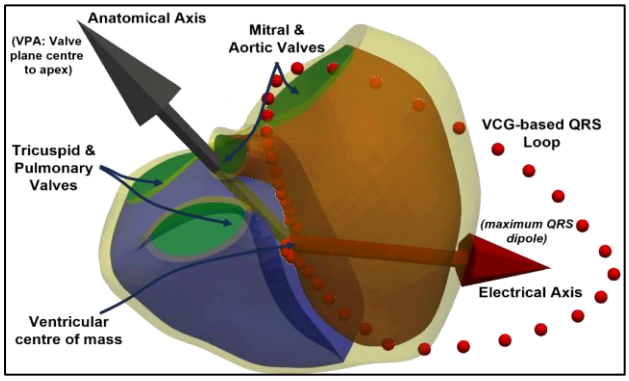

Figure 3. Biventricular geometry with both axes.

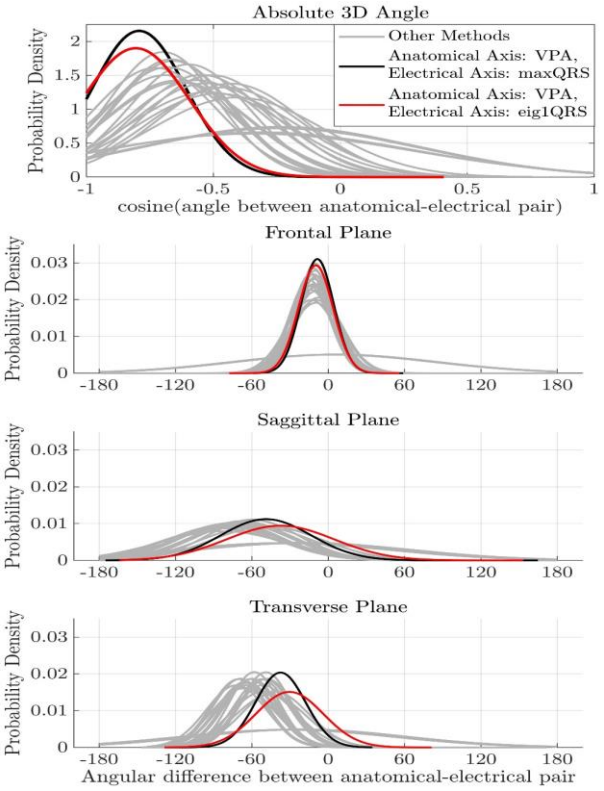

Figure 4. 3D and 2D angular distributions. *Levene's test confirmed heterogeneity of the distributions at p = 0.05*.

anatomical axis angles was markedly lower than that of the electrical and the angular difference. While the angular difference was primarily influenced by the electrical axis (marginal distributions), the anatomical impact is discernible when observing the density estimates, due to their insight into underlying distributions.

4. Discussion

The proposed standard for defining the anatomical axis is the VPA (valvular plane centre to apex), while for the electrical axis, it is suggested to use the maxQRS (max QRS dipole magnitude in VCG). This proposal is derived from an assessment of a cohort without cardiovascular disease based on maximal alignment criteria.

In terms of anatomical orientation, the VPA definition clearly outperformed the other four (see Figure 2). This definition combines two components that empirically showed to be a strength: (i) specific anatomical points selection, e.g. apex or valve centre, rather than the identification of the axis of inertia, i.e. with PCA, and (ii) the inclusion of the right ventricle rather than LV only based orientations (the valvular plane centroid allows a weighted contribution from both ventricles). This finding highlights that, although the LV's contribution to the QRS is dominant due to its larger mass, there are spatial changes that are best captured by also accounting for the RV.

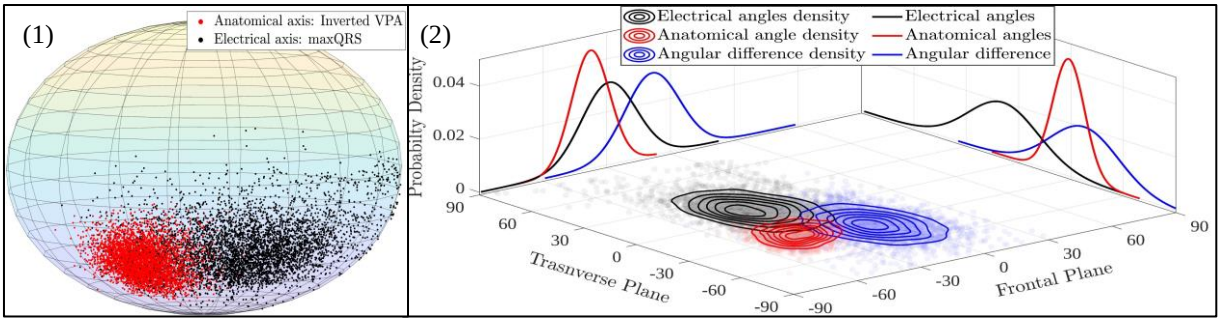

Figure 5. (1) Axes spherical distribution. (2) Bivariate (Frontal & Transverse) probability density distributions of electrical and anatomical angles, and their differences (normal-fitted marginal distributions and kernel density estimation contours).

Regarding electrical orientation, maxQRS and eig1QRS definitions were the most aligned to the anatomical based on the two metrics investigated (maxQRS for the angular metric, Figure 4, and eig1QRS for the least squares (LS) metric, Figure 2). While maxQRS reflects the maximum dipole magnitude, eig1QRS, captures the shape and spread of the QRS loop, offering a more extensive/holistic representation of depolarisation. The discordance between the two metrics stems from their underlying principles: the angular metric emphasises spatial orientations, whereas the LS metric considers the linear correlation between axes. Ultimately, maxQRS is suggested as the optimal definition due to the angular metric's capacity to represent non-linear relationships, as opposed to the linear constraint of the LS approach, and its ability to capture rotational patterns. Moreover, maxQRS offers more robust implementation in future studies, as eig1QRS relies on the detection of QRS onset and offset.

Once the definitions of the axes were set, the inspection of the population characteristics revealed a wider electrical angle spread, suggesting a wider variability of both mechanistic factors and uncontrolled variables influencing cardiac depolarization. The seemingly under-constrained electrical angle distributions could be due to ECG morphology being influenced by conduction-related factors, such as fibre orientation within the myocardium, technical variables like electrode placement, and anatomical structure [9]. In contrast, the narrower spread of the anatomical axis can be attributed to the cardiac-torso anatomy being robustly captured by an MRI scan.

While the present study provides valuable insights into axes coupling, the influence of age, BMI, and sex on the observed spatial relationships should be explored. This is in addition to exploring the impact of pathologies that would impact either axis, such as cardiomyopathy or bundle branch blocks. The repolarisation axis could provide further insights into the relationship between cardiac electrical dynamics and anatomy.

Acknowledgments

This work was supported by the CDT in Digital Twins for Healthcare, and the Wellcome/EPSRC Centre for Medical Engineering (WT203148/Z/16/Z). This research has been conducted using data from UK Biobank, a major biomedical database (application ID 88878).

References

[1] U. C. Nguyên *et al.*, 'An in-silico analysis of the effect of heart position and orientation on the ECG morphology and vectorcardiogram parameters in patients with heart failure and intraventricular conduction defects', *J Electrocardiol*, vol. 48, no. 4, pp. 617–625, Jul. 2015.

[2] A. Mincholé, E. Zacur, R. Ariga, V. Grau, and B. Rodriguez, 'MRI-Based Computational Torso/Biventricular Multiscale Models to Investigate the Impact of Anatomical Variability on the ECG QRS Complex', Front Physiol, vol. 10, Aug. 2019.

[3] H. Engblom *et al.*, 'The relationship between electrical axis by 12-lead electrocardiogram and anatomical axis of the heart by cardiac magnetic resonance in healthy subjects', *Am Heart J*, vol. 150, no. 3, pp. 507–512, Sep. 2005.

[4] W. Einthoven, 'The Different Forms of the Human Electrocardiogram and Their Signification.', *The Lancet*, vol. 179, no. 4622, pp. 853–861, Mar. 1912.

[5] F. Isensee, P. F. Jaeger, S. A. A. Kohl, J. Petersen, and K. H. Maier-Hein, 'nnU-Net: a self-configuring method for deep learning-based biomedical image segmentation', *Nature Methods 2020 18:2*, vol. 18, no. 2, pp. 203–211, Dec. 2020.

[6] C. Mauger *et al.*, 'Right ventricular shape and function: Cardiovascular magnetic resonance reference morphology and biventricular risk factor morphometrics in UK Biobank', *Journal of Cardiovascular Magnetic Resonance*, vol. 21, no. 1, pp. 1–13, Jul. 2019.

[7] S. Q. Duong *et al.*, 'Quantitative Prediction of Right Ventricular Size and Function From the ECG', *J Am Heart Assoc*, vol. 13, p. 31671, Jan. 2023.

[8] J. A. Kors, G. Vanherpen, A. C. Sittig, and J. H. Van Bemmel, 'Reconstruction of the Frank vectorcardiogram from standard electrocardiographic leads: diagnostic comparison of different methods', *Eur Heart J*, vol. 11, pp. 1083–1092, 1990, Accessed: Oct. 30, 2023.

[9] B. J. A. Schijvenaars, G. van Herpen, and J. A. Kors, 'Intraindividual variability in electrocardiograms', *J Electrocardiol*, vol. 41, no. 3, pp. 190–196, May 2008.

Address for correspondence:
Mohammad Kayyali
4th Floor North Wing, St Thomas' Hospital, London SE1 7EH
mohammad.kayyali@kcl.ac.uk